Nuclear Physics B167 (1980) 454–478

QCD PREDICTIONS FOR FOUR-JET FINAL STATES IN e^+e^- ANNIHILATION

A. ALI, J.G. KÖRNER, Z. KUNSZT[1] and E. PIETARINEN
Deutsches Elektronensynchrotron DESY, Hamburg, Germany

G. KRAMER, G. SCHIERHOLZ and J. WILLRODT
II. Institut für Theoretische Physik der Universität Hamburg, Germany*

Received 19 November 1979

We have calculated the four-jet production processes $e^+e^- \to q\bar{q}gg$ and $e^+e^- \to q\bar{q}q\bar{q}$ to lowest-order QCD perturbation theory. We find that $(q\bar{q}q\bar{q})$ production is small compared to the dominant process $e^+e^- \to q\bar{q}gg$ which can in part be traced to the fact that the latter process is more singular as the 2- and 3-jet phase-space limits are approached. We present differential 4-jet acoplanarity distributions and compare them with non-perturbative acoplanarity distributions at maximum PETRA and PEP energies. Leading log cross-section formulae are derived for various cut-off procedures and are compared to the results of our numerical integrations. We also present results on associated heavy quark production in e^+e^- annihilation.

1. Introduction

It is generally believed that quantum chromodynamics (QCD), the gauge theory of coloured quarks and gluons, is the underlying theory of strong interactions. This theory is closely related to the best known field theory, quantum electrodynamics (QED), which is an abelian gauge theory. QCD, on the contrary, is a non-abelian gauge theory with the gauge group $SU(3)_{(colour)}$. Hence the gluons have colour and thus couple to each other.

Although QCD is well-defined as a field theory it is not without problems. For example, it is not known yet whether QCD confines quarks and gluons and whether one is able to predict the spectrum of existing hadrons. However, at very high energy or momentum transfer q^2 the coupling constant $\alpha_s(q^2)$ decreases, with increasing q^2, due to asymptotic freedom. As was emphasized by many authors, this allows one to calculate those parts of a process involving high q^2 by the use of perturbation theory. On this basis a large number of cross sections were calculated which serve as tests of QCD.

One of the most interesting predictions of QCD is the existence of hadronic jets in e^+e^- annihilation resulting from the primordial production of quarks and gluons [1].

[1] On leave from L. Eötvös University, Budapest.

* Supported by Bundesministerium für Forschung und Technologie.

At moderate energies this means basically a two-jet final state coming from the lowest-order diagram $e^+e^- \to q\bar{q}$, while gluons radiating off the quark and antiquark are hidden in the non-perturbative jet spread. Experiments at SPEAR and DORIS have confirmed this picture [2]. Quarks and gluons are thought to materialize into jets in which the particles have limited transverse momentum $\langle p_T \rangle_{\text{nonpert}} \simeq 0.3$ GeV. In contrast to this, the mean transverse momentum of a gluon emitted from a quark or antiquark grows with increasing energy like $\langle p_T^2 \rangle \approx q^2/\ln q^2$ [3]. Hence the production of quarks *and* gluons becomes visible at high enough energy as final states containing three or more jets. In the meantime there is convincing evidence for three jets at PETRA from the Tasso and Mark J collaborations [4]. Whether the properties of these three-jet events agree with the theoretical expectations will be seen in the future. Many QCD predictions for quark-antiquark-gluon ($q\bar{q}g$) final states have been reported [3, 5]. QCD shows its full gauge structure, however, only in second- or higher-order perturbation theory (order $\geqq \alpha_s^2$) where the triple-gluon coupling comes in.

In second order we will be led to four-jet final states: $e^+e^- \to q\bar{q}gg$ and $e^+e^- \to q\bar{q}q\bar{q}$. Some aspects of the four-quark final state have been studied in ref. [6]. We shall present our results in terms of invariant jet measures as thrust, acoplanarity, etc., since these variables are least sensitive to the details of the fragmentation of quarks and gluons into hadrons which we do not treat in our calculation. For the 4-jet calculation, acoplanarity is a very useful variable since four-jet events stand out against two- and three-jet final states by having a non-vanishing acoplanarity A [7]. Thus $d\sigma/dA$ is the canonical quantity to analyse as it allows one to cut off the dominant two- and three-jet events experimentally. Of course to consider events with non-vanishing A does not eliminate the two- and three-jet background completely since these events have some finite A through the non-perburbative jet spread near $A \simeq 0$. With an appropriate cut on A one can reduce this non-perturbative background contribution and thereby enhance the true QCD perturbative contribution. Of a similar nature are background effects originating from the weak decay of heavy quarks [8].

Other tests of the three-gluon coupling have been proposed [9]. Some of them are concerned with the study of 3g decays of $Q\bar{Q}$ resonances at higher energies. In a recent note we presented the results of the acoplanarity distribution $d\sigma/dA$ for all four-jet final states and compared them to the non-perturbative background [10]. In this paper we report the details of the calculations, their interpretation and the influence of background effects. In particular we consider the final states $q\bar{q}gg$ and $q\bar{q}q\bar{q}$ separately and for the latter process we consider particular flavour final states using massive quarks which might be of use for comparison with future experimental data.

The outline of the paper is as follows. In sect. 2 we describe the framework of our calculations and give predictions for $d\sigma/dA$, $d\sigma/dT$ and $d\sigma/d\tilde{S}$ where $\tilde{S}$ denotes sphericity. In sect. 3 we study the most singular region of the four-jet distribution

using various variables and cut-off procedures. Some results for massive four-quark states are reported in sect. 4. Finally, in sect. 5 we summarize our conclusions.

Technical details are relegated to the appendices. Appendix A contains the complete cross-section formula for the process $e^+e^- \to q\bar{q}gg$. In appendix B we analytically calculate the leading log contributions to the two cross sections for various cut-off procedures. In appendix C we present formulae for the 6 structure functions that occur in these processes and comment on more stringent tests of four-jet states using angular correlations and asymmetries similar to the earlier work on three-jet final states [11].

2. Acoplanarity distribution of four-jet states

To order α_s^2 the four-jet cross section is given by the two sets of diagrams shown in fig. 1 which correspond to the final (jet) states

$$e^+e^- \to q(p_1)\bar{q}(p_2)g(p_3)g(p_4)\,, \tag{2.1}$$

$$e^+e^- \to q(p_1)\bar{q}(p_2)q(p_3)\bar{q}(p_4)\,. \tag{2.2}$$

The p_i denote the momenta of the produced particles, quarks, antiquarks or gluons. Throughout this section the quarks are assumed to be massless. The differential cross section is given by

$$d\sigma = \frac{e^4}{(2\pi)^8 2q^6}\{p_+, p_-\}^{\mu\nu} \prod_{i=1}^{4} \frac{d^3p_i}{2p_{i0}}\,\delta^{(4)}\left(p_+ + p_- - \sum_{k=1}^{4} p_k\right) H_{\mu\nu}\frac{1}{N_s}\,, \tag{2.3}$$

where $q = p_+ + p_-$. For unpolarized beams the lepton tensor is:

$$\{p_+, p_-\}^{\mu\nu} = p_+^\mu p_-^\nu + p_-^\mu p_+^\nu - g^{\mu\nu}\tfrac{1}{2}q^2\,. \tag{2.4}$$

The hadron tensor $H_{\mu\nu}$ contains summations over the final spin, colour and flavour states including the appropriate quark charge factors $\frac{1}{9}$ or $\frac{4}{9}$. N_s is a statistical factor due to the identity of final-state particles which is 2 for (2.1) and 4 for (2.2). An equivalent procedure would be to integrate only over half and quarter of phase space, respectively, when calculating integrated quantities. As an example we have written down the formulae for $H_{\mu\nu}$ for $e^+e^- \to q\bar{q}gg$ in appendix A.

The differential cross section (2.3) depends on five independent "hadronic" variables describing the 4-jet final state which one could choose as x_1, x_2, x_3, x_{12} and x_{13}, where

$$x_i = \frac{2|\boldsymbol{p}_i|}{\sqrt{q^2}}\,, \qquad x_{ij} = \frac{2|\boldsymbol{p}_i + \boldsymbol{p}_j|}{\sqrt{q^2}}\,, \tag{2.5}$$

and two angle variables θ and χ which describe the orientation of the "hadronic" 4-jet event relative to the leptonic beam direction. We have used a Monte Carlo routine to integrate over the angle variables and 4 of the 5 hadronic variables leaving

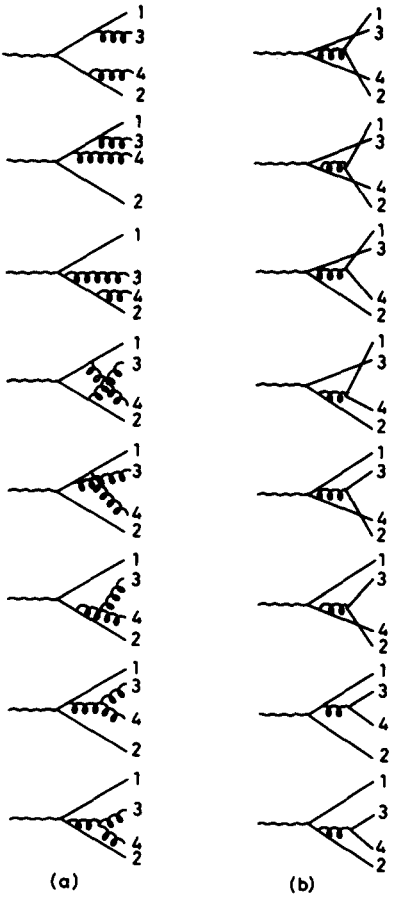

Fig. 1. Tree diagrams for four-jet production (a) $q\bar{q}gg$ and (b) $q\bar{q}q\bar{q}$.

us with a differential distribution in one variable which we choose as the acoplanarity defined by [7]

$$A = 4 \min \left\{ \frac{\sum_i |\boldsymbol{p}^i_{\text{out}}|}{\sum_i |\boldsymbol{p}_i|} \right\}^2 . \tag{2.6}$$

The sum in (2.6) runs over all particles in the final state and p^i_{out} is measured perpendicular to a plane chosen to minimize A. We consider the variable A first. Four jets, as compared to three- and two-jet final states, are characterized by a non-vanishing A. Of course, instead of A, other variables can be chosen, like thrust T or sphericity $\tilde{S}$. However, differential T and $\tilde{S}$ distributions are not singularity free at the tree-graph level since the remaining phase-space integrations include singular configurations of quarks and gluons. Therefore, from this point of view, it is natural to study the dependence of the cross section on A first. We show the A distribution

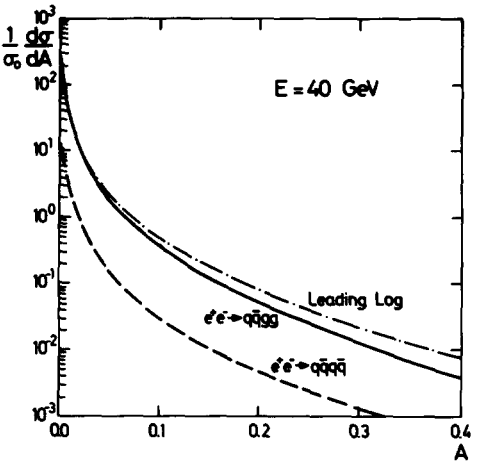

Fig. 2a. $d\sigma/dA$ for $e^+e^- \to q\bar{q}gg$ (full curve), $e^+e^- \to q\bar{q}q\bar{q}$ (dashed curve) and $e^+e^- \to q\bar{q}gg$ in the leading log approximation (dashed-dotted curve).

$d\sigma/dA$ normalized to the zeroth-order cross section $\sigma_0 = 4\pi\alpha^2 \sum_a Q_a^2/q^2$ for $\sqrt{q^2} = E = 40$ GeV in fig. 2a. Since the q^2 dependence of $\sigma_0^{-1}\, d\sigma/dA$ is determined by $\alpha_s^2(q^2)$ the result can easily be extrapolated to other energies by the known q^2 dependence of $\alpha_s(q^2)$ where

$$\alpha_s(q^2) = 12\pi \Big/ \left(33 - 2N_f\right) \ln \frac{q^2}{\Lambda^2}\,. \tag{2.7}$$

We take $N_f = 6$ and $\Lambda = 0.5$ GeV.

The differential cross section $d\sigma/dA$ diverges for $A \to 0$. For $e^+e^- \to q\bar{q}gg$ the leading log behaviour is

$$\sigma_0^{-1} \frac{d\sigma}{dA} = \frac{8}{9}\left(\frac{\alpha_s}{\pi}\right)^2 \frac{1}{A} |\ln A|^3 \tag{2.8}$$

as $A \to 0$ (see appendix B). The leading log formula can be seen to give a good description of the differential A distribution up to rather large A values. For four massless final-state particles A is bounded between 0 and $\frac{2}{3}$. The maximal A value occurs for the configuration where the 4 momenta point from the center of a tetrahedron [with side length $(\frac{1}{6}q^2)^{1/2}$] to its 4 corners which gives $A = \frac{2}{3}$ according to eq. (2.6). We do not show the corresponding comparison for $e^+e^- \to q\bar{q}q\bar{q}$ where the leading behaviour is $\sim A^{-1} \ln^2 A$. The latter cross section can be seen to be $\simeq 10$ times smaller than the former over most of the region of A.

The comparison with $d\sigma/dA$ for non-perturbative 2-jet production calculated in a Feynman–Field model [12] is presented in fig. 2b. This distribution which includes also weak decay effects of c and b quarks [13] is still rather broad at $\sqrt{q^2} = 40$ GeV. The input p_T for the Feynman–Field model is $\sigma_q = \langle p_T^2 \rangle^{1/2} = 0.25$ GeV. The average A for this non-perturbative 2-jet distribution is calculated to be $A_{\text{nonpert}} = 0.04$. This

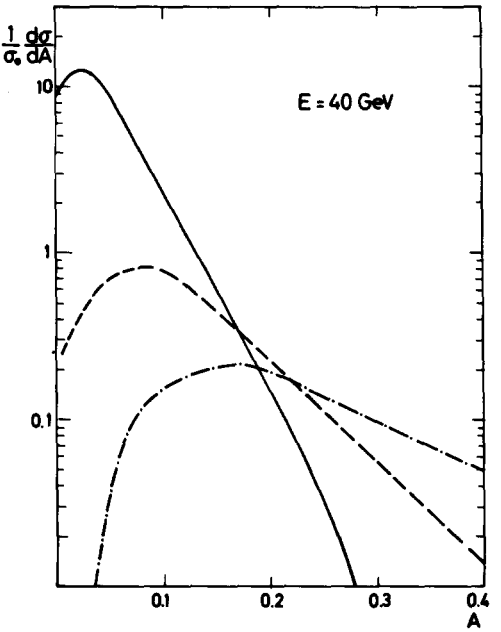

Fig. 2b. $d\sigma/dA$ for non-perturbative two-jet contribution in a Feynman–field type model [13] (full curve), for $e^+e^- \to q\bar{q}g$ with quark and gluon fragmentation (dashed curve) and for $e^+e^- \to q\bar{q}gg + q\bar{q}q\bar{q}$ with quark and gluon fragmentation (dashed-dotted curve).

is a much larger value than the value assumed in our earlier work [10]* ($A_{\text{nonpert}} = 0.01$) which was based on the estimate [3 (4th ref.)]

$$\langle A\rangle_{\text{nonpert}} = \frac{16}{\pi^2 q^2}\langle n-2\rangle^2 \langle p_T^2\rangle_{\text{nonpert}}\,, \tag{2.9}$$

where we used $\langle n\rangle = 1.5\ (2+0.7\ln q^2)$ for the total multiplicity as extracted from low-energy data. The larger value of $\langle A\rangle_{\text{nonpert}}$ in the Feynman–Field model is mostly due to higher particle multiplicities in this model for higher energies which agrees much better with the new high-energy data [4] than the naive extrapolation of the low-energy data. Some increase of $\langle A\rangle_{\text{nonpert}}$ is also due to the jet broadening from weak decays of b quarks. Additional background comes from fragmentation corrections to the three-jet cross section $q\bar{q}g$. Although this contribution is reduced in magnitude, if compared to the 2-jet contribution, by a factor $\simeq 10$ it is broader than the 2-jet contribution. The 3-jet contribution is calculated with a thrust cut-off $T_c = 0.9$ motivated by demanding $\sigma_{q\bar{q}g}(T_c)/\sigma_0 \simeq \alpha_s$. Instead to compare with the tree-graph prediction $d\sigma/dA$ of fig. 2a we have supplemented the 4-jet contributions with quark and gluon fragmentation also. The result for any acoplanarity cut-off $A_c = 0.05$ (for a justification see below) is shown in fig. 2b also. The normalization of

* Note that the differential A distribution shown in [10] is for the sum of the two processes. The scale of the ordinate axis in the relevant fig. 2 of [10] is in error and should be multiplied by a factor 250 to obtain the correct normalization.

the three curves in fig. 2b is such that the area under the sum of the three contributions is one. The relative normalization of the 2-jet, 3-jet and 4-jet cross sections is 0.82, 0.13 and 0.05.

Fig. 2b shows that A must be larger than 0.3 before the 4-jet contribution exceeds the background from $q\bar{q}g$. Therefore this would be the region where the perturbative 4-jet contribution can be tested. In this region $(1/\sigma_0)\,d\sigma/dA$ dropped down by two orders of magnitude. Thus high-statistics experiments are needed to see the α_s^2 terms. However, applying a restrictive T-cut would eliminate almost the total two-jet signal without losing any four-jet events. For example, considering only events with $T \leqq 0.75$ leads to $\sigma(2\text{-jet}):\sigma(3\text{-jet}):\sigma(4\text{-jet}) = 0.02:0.66:0.32$, so that the 4-jet term is very much enhanced.

Because of the singularity for $A \to 0$ [see (2.8)] the differential cross section $d\sigma/dA$ is not integrable over A. This is to be expected because of the infrared singularities associated with collinear and soft emission of quarks, antiquarks and gluons in (2.1) and (2.2).

Of course, when calculating the total cross section to order α_s^2, these singularities cancel against the corresponding singularities of the one- and two-loop virtual contributions. Due to the singular behaviour of $d\sigma/dA$ as $A \to 0$ the differential distribution should be considered to be reliable only for values of A above some cut-off A_c. Integrating $d\sigma/dA$ from $\frac{2}{3}$ to A_c one obtains a cut-off dependent 4-jet cross section $\sigma(A_c)$ which is shown in fig. 3. A cutoff value for which $\sigma(A_c)/\sigma_0 \simeq \alpha_s^2 \simeq 0.04$ should be considered a reasonable choice above which a perturbatively calculated $d\sigma/dA$ can be trusted. From fig. 3 this corresponds to $A_c = 0.07$.

We also show in fig. 3 the ratio of four-jet to three-jet production as a function of A_c. The three-jet cross section is computed with a thrust cut-off at $T_c = 0.9$. We see that this ratio is quite large if the A cut-off is chosen in the vicinity of 0.1.

Since only the tail of the A distribution is a genuine prediction of perturbative QCD, the QCD prediction for the average acoplanarity $\langle A \rangle$ may not provide a realistic measure of perturbative QCD since $\langle A \rangle$ obtains non-negligible contributions from the region $A \simeq 0$ where the 2nd order calculation can no longer be trusted. For this reason the 2nd-order QCD value for $\langle A \rangle$ as calculated in our earlier publication [10] must be considered to be an overestimate and should not be naively compared to $\langle A \rangle_{\text{nonpert.}}$ Higher moments $\langle A^n \rangle$ would be better measures of the QCD contribution since the region $A \simeq 0$ is de-emphasized. Thus measurements of the energy dependence of $\langle A \rangle$ which is free of the above difficulty are important. Whereas the non-perturbative background has a $(\ln^2 E/E^2)$ energy dependence, one would have $(1/\ln^2 E)$ for the QCD contribution.

In order to avoid the A region close to 0 it may be more sensible to compute an average acoplanarity with a lower cut-off A_c, i.e.,

$$\langle A \rangle_{A_c} = \sigma_0^{-1} \int_{A_c} dA\, A \frac{d\sigma}{dA}. \tag{2.10}$$

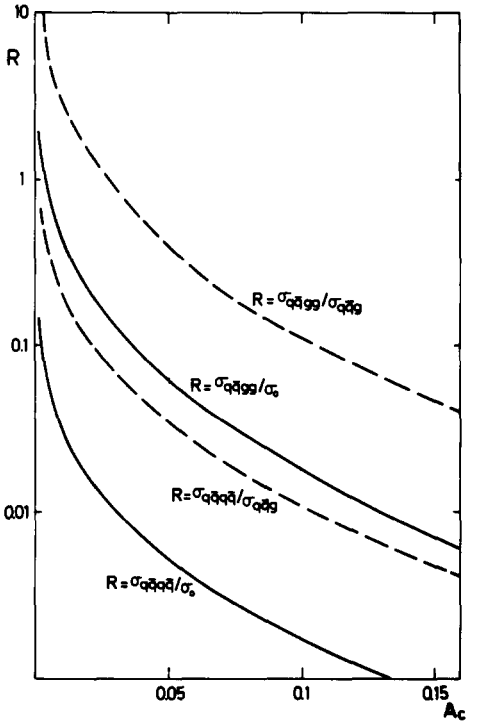

Fig. 3. Integrated four-jet cross section as a function of the acoplanarity cut-off A_c for $e^+e^- \to q\bar{q}gg$ and $e^+e^- \to q\bar{q}q\bar{q}$ separately. Ratio of σ (four-jet) to σ (three-jet) as a function of A_c. The $q\bar{q}g$ cross section is cut off at $T_c = 0.9$.

In table 1 we have listed the result of such a truncated average for several values of A_c. These numbers could be compared to experimental $\langle A \rangle_{A_c}$ defined in the same interval. Note that the definition of $\langle A \rangle_{A_c}$ in (2.10) is unconventional since the average value does not lie in the interval in which the distribution is averaged. In order to have an idea of how different cut-off choices affect the phase-space integration region we have listed in table 2 phase-space fractions for various choices of A_c and (δ, ε).

The subset of four-jet final states consisting of four quark jets has much smaller cross section than the $q\bar{q}gg$ jets. For all relevant cut-off values A_c the ratio of $\sigma(q\bar{q}q\bar{q})/\sigma(q\bar{q}gg)$ is roughly 0.1. (see fig. 2a). One can check that $\sigma(q\bar{q}gg)$ is

TABLE 1
$\langle A \rangle$ as a function of A_c

A_c	$\langle A \rangle$
0.01	0.013
0.02	0.010
0.05	0.0057

TABLE 2
Phase-space fraction as a function of A_c

A_c	fraction (%)	($\delta = 5°$, ε)	fraction (%)
0	100	0	100
0.001	75	0.001	93
0.005	57	0.005	90
0.01	46	0.01	88
0.05	20	0.05	67
0.10	9.4	0.1	40
0.15	4.9	0.15	16

well-described by the leading log formula up to fairly high values of A_c as can be expected from the accuracy of the leading log formula for the differential distribution. However, $\sigma(q\bar{q}q\bar{q})$ is substantially below the leading log contribution even for very small A_c values and does not even show the $|\ln^3 A_c|$ dependence of the leading log formula (see appendix B). We take this as an indication that non-leading log contributions are still important in this case for the A_c region under consideration.

One of the aims of our investigation was to see how large the influence of the three-gluon coupling is. In some sense this is an ill-defined question since on the one hand the relative contribution of the three-gluon coupling depends on the gauge choice and on the other hand theories with only global SU(3) symmetry are not renormalizable (although for our tree-diagram renormalization this is not relevant). Therefore we compare to an abelian theory (i.e., QED with massless and colourless quarks) which is gauge invariant in itself. For such a theory we get for the $q\bar{q}gg$ cross section

$$\sigma(q\bar{q}gg, \text{QED}) \simeq 0.15\sigma(q\bar{q}gg, \text{QCD}) . \tag{2.11}$$

From (2.11) we would estimate the effect of coloured gluons in the four-jet cross section to be 85%. Of course, if we take into account that $\sigma_0(\text{QED}) = \frac{1}{3}\sigma_0(\text{QCD})$ corresponding to an abelian theory with coloured quarks and colour-singlet gluons, and further, if we normalize the abelian coupling α_s to $e^+e^- \to q\bar{q}g$ (α_s (abelian) $= \frac{4}{3}\alpha_s$ (non-abelian)), the relative $q\bar{q}gg$ rate would be multiplied by $\frac{16}{3}$. In this case the relative weight of $q\bar{q}q\bar{q}$ is enhanced by a factor 8, approximately, compared to the QCD case.

Finally we present the dependence of the four-jet cross section on some other variables. As we mentioned already, the four-jet cross section depends on five variables so that multidifferential cross sections such as, for example, $d^2\sigma/dA\, dT$ or $d^2\sigma/dA\, d\tilde{S}$ could be measured in principle. As this requires high-statistics data which will not be available for some time to come, we do not present results on these two-dimensional distributions but integrate these over A. As discussed earlier, the singular region $A \to 0$ has to be excluded in this integration. In figs. 4 and 5 we present differential thrust and sphericity distributions for an acoplanarity cut $A_c = 0.05$. The

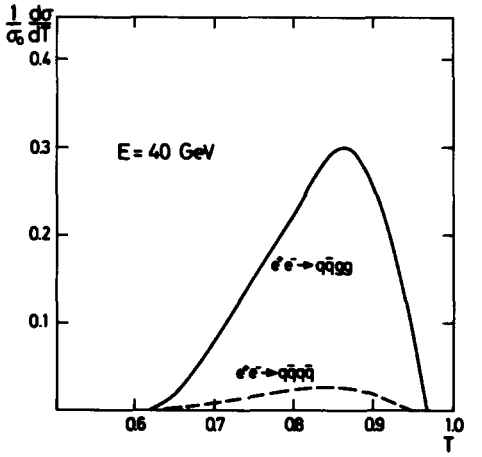

Fig. 4. Differential thrust distribution with acoplanarity cut $A_c = 0.05$. Normalization described in text.

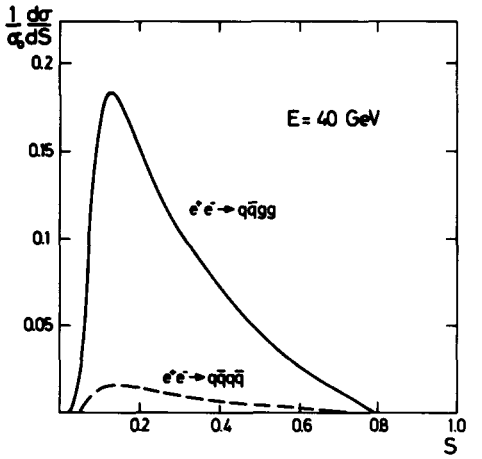

Fig. 5. Differential sphericity distribution with acoplanarity cut $A_c = 0.05$. Normalization described in text.

curves are normalized in such way, that the area under the curve gives the integrated cross sections in fig. 3*.

It is clear that the tests of four-jet behaviour in QCD presented so far are rather limited. They presumably test very little of the vector character of the gluons and finer details of the three-gluon coupling. For this purpose angular correlations and asymmetries of the final jets would be much more suitable.

Such tests will require very high statistics and are not likely to become relevant in the initial stages of the PETRA and PEP physics programs. Nevertheless we discuss

* The lower kinematical limit on T is $\sqrt{\frac{1}{3}}$.

some aspects of these questions in appendix C in order to provide a rough idea on the physics potential of such measurements.

3. (δ, ε) cuts for $e^+e^- \to q\bar{q}gg$

In sect. 2 we demonstrated that the leading log formula for the differential A distribution gives a surprisingly good account of the full 2nd-order calculation up to quite large A values. In this section we discuss the accuracy of the (integrated) leading log formula using the angle-energy cuts (δ, ε) as introduced by Sterman and Weinberg. We shall concentrate on the case $e^+e^- \to q\bar{q}gg$ since it is the dominant 2nd-order process.

From the explicit expressions in appendix B it is clear that the most singular configuration corresponds to the gluons becoming soft and collinear with the quark (or antiquark). Thus the boundary of the most singular phase-space region is defined by $\theta_{q(\bar{q})g} \geqq 2\delta$ and $|\boldsymbol{p}_g| \geqq \varepsilon\sqrt{q^2}$. When studying the dependence of the cross section on angle-energy cut parameters one has to, however, also cut out regions of phase space which contain non-leading singularities, such as those arising from the 3-gluon vertex $g \to gg$ when the two gluons become collinear. We thus define our cuts as

$$\theta_{ij} \geqq 2\delta\,, \tag{3.1a}$$

$$|\boldsymbol{p}_i| \geqq \varepsilon\sqrt{q^2}\,, \tag{3.1b}$$

for $i, j = 1, \ldots 4$, i.e., we cut on the topology of events with no distinction between quarks and gluons. Simple geometrical arguments show that these conditions are sufficient to populate $\frac{5}{6}$ of the boundary of the most singular phase-space region [the reduction factor of $\frac{5}{6}$ is due to the fact that (3.1a) excludes the collinear two-gluon configuration]. Of course these conditions also exclude events not on the boundary of the most singular region which is, however, of no consequence in the leading log comparison.

In order to investigate the quality of the leading log cross-section formula we have done a "high-statistics" Monte Carlo cross section run using variable (δ, ε) cuts as defined in eq. (3.1). In fig. 6 we exhibit the ε dependence of the 4-jet cross section for various δ values.

We also present our results in terms of the ratio

$$R(\delta, \varepsilon) = \sigma_{q\bar{q}gg}(\delta, \varepsilon)/\sigma^{LLA}_{q\bar{q}gg}\,, \tag{3.2}$$

where

$$\sigma^{LLA}_{q\bar{q}gg}/\sigma_0 = \frac{5}{6}\frac{128}{9}\left(\frac{\alpha_s}{\pi}\right)^2 \ln^2\delta \ln^2 2\varepsilon \tag{3.3}$$

[see (B.5)] includes the above factor $\frac{5}{6}$. The result of this comparison is shown in fig. 7 (dotted lines) for $\delta = 5°$ and $1°$. From the curves in fig. 7 it is clear that one has to

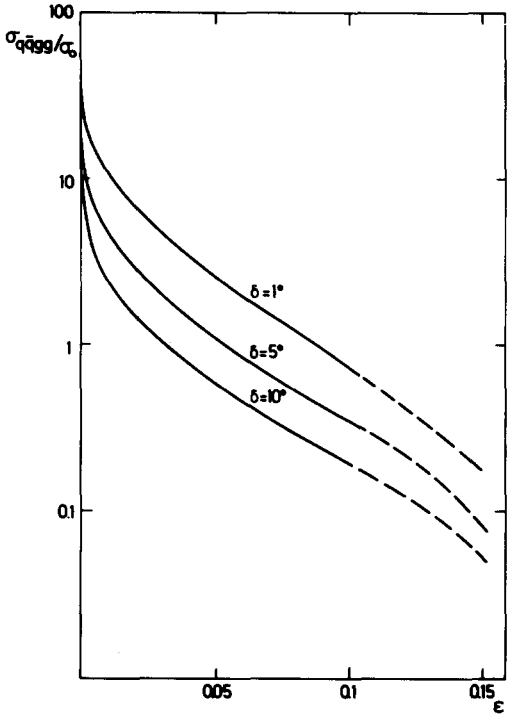

Fig. 6. δ and ε dependence of ($q\bar{q}gg$) cross section. $E = 40$ GeV.

choose rather small values of δ and ε before the leading log formula (3.3) approaches the result of the Monte Carlo integration. This shows that non-leading terms are not negligible.

The fact that $R(\delta, \varepsilon)$ tends to zero as $\varepsilon \to \frac{1}{4}$ in fig. 7 can be traced back to the energy cut which gives $\sigma_{q\bar{q}gg}$ $(\delta, \varepsilon = 0.25) = 0$ as the kinematical limit of energy equidistribution is reached. The presence of this kinematical zero tends to distort $R(\delta, \varepsilon)$ as $\varepsilon \to 0.25$. Therefore we have also included in fig. 7 the comparison to a leading log formula with the same kinematical zero by adding a non-leading contribution to (3.3) such that $\ln 2\varepsilon \to \ln 4\varepsilon$. The agreement with the exact calculation becomes worse. One sees, however, that the effect of the spurious zero at $\varepsilon = 0.25$ is weakened. We have not systematically searched for improvements of the leading log formula by adding suitable non-leading terms.

Judging from the accuracy of the leading log formula for the acoplanarity distribution discussed in sect. 2 as compared to the (δ, ε) leading log formula, one must conclude that non-leading terms do not play such an important role in the former case as in the latter. In particular the leading log formula for $\sigma(A_c)$ is still quite good for values of A_c for which $\sigma(A_c)/\sigma_0 \ll 1$ where 2nd-order perturbation theory can still be trusted. This is not true for the (δ, ε) case, where the leading log result shows larger deviations from the calculated cross section in the (δ, ε) region

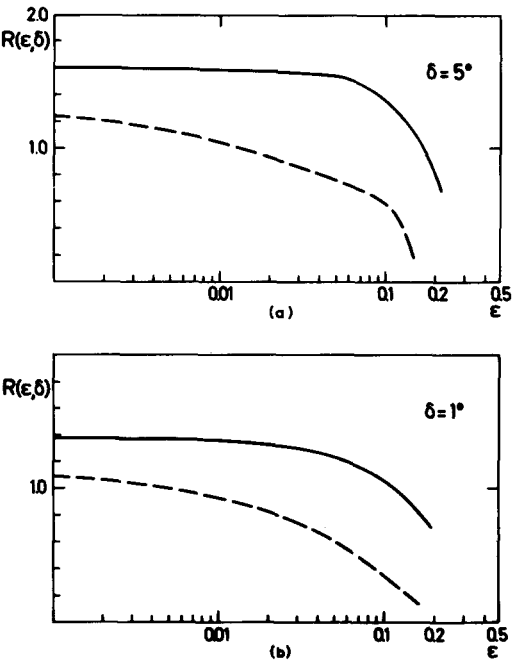

Fig. 7. δ and ε dependence for ($q\bar{q}gg$) cross section divided by leading log cross section. $E = 40$ GeV. The dashed curve is the case where $\ln 2\varepsilon$ is replaced by $\ln 4\varepsilon$.

where $\sigma(\delta, \varepsilon)/\sigma_0 \ll 1$. On the other hand, one should not rely on cross-section estimates based on too small A and (δ, ε) cuts even if the leading log accuracy is good if the cuts corresponds to $\sigma(\text{cuts})/\sigma_0 > 1$. In such a case the finite-order perturbation theory calculation does not make sense any longer. In this context we would like to remark that the estimate of the ($q\bar{q}q\bar{q}$) production cross section of de Grand et al. [3] based on an invariant mass cut $\hat{\varepsilon} = 0.01$ must be considered to be too large. They used eq. (B.11) and $N_f = 4$ to obtain $\sigma_{q\bar{q}q\bar{q}}/\sigma_0 \simeq 1.4$ which is clearly too large for perturbation theory to be valid. This may be ameliorated by the observation that the leading log formula $\sigma_{qqq\bar{q}}(\hat{\varepsilon})^{\text{LLA}}$ (B.11) is a substantial overestimate of the true cross section even for this $\hat{\varepsilon}$ value which, however, leads to the same conclusion that the ($q\bar{q}q\bar{q}$) cross section given in [3] is an overestimate.

4. Massive four-quark production

Several authors have advocated the use of QCD perturbation theory to estimate associated new flavour production by calculating $e^+e^- \to q\bar{q}q\bar{q}$ for *massive* quarks with new flavours [15]. We have extended the calculations for massless quarks described in the previous sections to the massive quark case. It is clear that there is no need for an additional cut-off in the ($q\bar{q}q\bar{q}$) case since the massiveness of the quarks provide a natural cut-off.

TABLE 3
Relative rates for heavy quark production

E	$c\bar{c}c\bar{c}/c\bar{c}$	$c\bar{c}b\bar{b}/b\bar{b}$	$b\bar{b}b\bar{b}/b\bar{b}$
40	0.0052	0.0059	0.00029
80	0.0109	0.019	0.0019

In table 3 we present our results for the three cases (i) $e^+e^- \to c\bar{c}c\bar{c}$, (ii) $e^+e^- \to c\bar{c}b\bar{b}$ and (iii) $e^+e^- \to b\bar{b}b\bar{b}$, where we have used mass values $m_c = 1.6$ GeV and $m_b = 4.6$ GeV and energies of $\sqrt{q^2} = 40$ GeV and 80 GeV. The rates relative to the zeroth-order cross section σ_0 are extremely small. In this case σ_0 is calculated using massive quarks, i.e., $c\bar{c}$ in cases (i) and (ii) and $b\bar{b}$ in case (iii). For example, at $\sqrt{q^2} = 40$ GeV the $(c\bar{c}b\bar{b})$ production rate is only 0.5% of the $(c\bar{c})$ production rate. Our results agree with the numerical results of [15]. Note, though, that the leading log expression used in [15] for comparison is too large by a factor of two (see appendix B).

In the case of associated charm production ($e^+e^- \to c\bar{c}c\bar{c}$) our calculation is exact as against the corresponding one in ref. [15] since we include the full interference structure which is neglected in [15]. We found that the contribution of the interference term is indeed negligible at these energies. Since the interference terms contribute only at the non-leading log level one would like to infer from this that the leading log terms are already dominant at these energies. In this context the large discrepancy between the exact result and the leading log formula which still persists at higher energies remains a puzzle [15] (we have checked that even for $q^2/4m^2 = 10^5$, $\sigma^{\mathrm{LLR}}/\sigma \simeq 1.9$ with a Monte Carlo integration error of 15%).

In our calculations we assumed the strong coupling constant α_s to be determined by the energy $\sqrt{q^2}$. With massive quarks the choice of α_s is not unambiguous and other energy scales could become relevant, such as $\sqrt{Q^2}$, where $\sqrt{Q^2}$ is the mass of the virtual gluon. The corresponding calculated cross sections would then be larger [15].

5. Summary and conclusion

We have calculated the four-jet production processes $e^+e^- \to q\bar{q}gg$ and $e^+e^- \to q\bar{q}q\bar{q}$ to lowest-order QCD perturbation theory. We have found that $(q\bar{q}gg)$ production dominates over $(q\bar{q}q\bar{q})$ production which can be in part traced to the fact that the first process is more singular in the limiting 2- and 3-jet configurations.

The calculated acoplanarity distribution at 40 GeV shows that the tail of the hard perturbative QCD processes should become visible above the non-perturbative 2-jet background for acoplanarity values $A \geqq 0.2$ and above the 3-jet background for $A \geqq 0.3$. If it should turn out that one is above $t\bar{t}$ threshold at 40 GeV, the interpretation of large-A events becomes more difficult due to the large-acoplanarity

t-background. One then has to either go to higher energies where the t-originated acoplanarity distribution shrinks or try to remove events with t-signature from the data sample.

We have found that the accuracy of the leading log formula for the acoplanarity distribution and the A_c-dependent ($q\bar{q}gg$) cross section is surprisingly good and can be used with some confidence to quickly estimate the 4-jet cross section. This is not true for the ($q\bar{q}q\bar{q}$) cross section where the leading log acoplanarity formula overestimates the true cross section by a substantial amount. The same statement holds true in the latter case for the other cut-off choices considered in the paper. We have calculated the rate of multiple heavy flavour production in the process $e^+e^- \to q\bar{q}q\bar{q}$ using massive quarks in the final state. The production rate was found to be quite small.

Finally we pointed out that measurements on the angular distribution of the 4-jet final states relative to the beam axis can provide even more powerful and detailed tests of the dynamics of interacting spin-$\frac{1}{2}$ quarks and spin-1 gluons.

Appendix A

Cross-section formula for $e^+e^- \to q\bar{q}gg$

We shall give an explicit cross-section formula only for the dominant subprocess $e^+e^- \to q\bar{q}gg$. For this purpose we introduce the following notation:

$$\begin{aligned} s &= p_3 \cdot p_4\,, & x &= p_1 \cdot p_3\,, \\ t &= p_2 \cdot p_3\,, & y &= p_1 \cdot p_4\,, \\ u &= p_2 \cdot p_4\,, & z &= p_1 \cdot p_2\,, \end{aligned} \tag{A.1}$$

and

$$(i,j)^{\mu\nu} = p_i^\mu p_j^\nu + p_i^\nu p_j^\mu - g^{\mu\nu} p_i \cdot p_j\,. \tag{A.2}$$

We can then write

$$H_{\mu\nu} = (4\pi\alpha_s)^2 \sum_{k=1}^{N_f} Q_k^2 \sum_{m \geqq n=1}^{8} A(m,n)_{\mu\nu}\,, \tag{A.3}$$

where (dropping the tensor indices ($\mu\nu$) except in $g_{\mu\nu}$)

$$A(1,1) = 64(3,4)/3xu\,,$$

$$\begin{aligned} A(2,1) = 64\{&-(2,2)(s+x) - u[(3,3)+(1,3)] + (1,2)(s+t) + (2,4)(t-x) \\ &+ (2,3)(s+2t+u+z) + (3,4)(t+z) + g_{\mu\nu}(sz - ty - ux)\}/3ux(s+x+y)\,, \end{aligned}$$

$$A(2,2) = 64\{(s+x)[(1,2)+(2,4)] - (2,3)y\}/3x(s+x+y)^2\,,$$

$$A(3,2) = 64\{-(1,1)[st+(t+u)(t+u+y+z)]-(3,3)uy-(4,4)xt$$
$$-(2,2)[sy+(x+y)(x+y+t+z)]+(3,4)(yt-sz+xu)$$
$$+(1,2)[s(y+x+u+t)+z(2z+3y+x+u+3t)+y(y+x+2u+4t)+2xu$$
$$+t(2x+u+t)]+(1,3)[z(s+z+y+t)-u(2y+x+u+t)]$$
$$+(2,3)[(z+y)(z+y+x+t)+y(s+u+t)]$$
$$+(1,4)[(z+t)(z+t+u+y)+t(s+y+x)]$$
$$+(2,4)[z(s+z+y+t)-x(y+x+u+2t)$$
$$+g_{\mu\nu}[s(-sz+ty-tz+ux+uz+xz-yz-2z^2)$$
$$+t(ty-ux+uy+xy+2xz+y^2+2yz)$$
$$+u(-ux-x^2-xy+2xz+2yz)]\}/3xu(s+x+y)(s+t+u)\,,$$

$$A(4,1) = 8z[(1,1)(s+u+t)+(2,2)(s+y+x)-(1,2)(2s+2z+y+x+u+t)$$
$$+(1,3)(u-y-z)+(1,4)(t-x-z)+(2,3)(y-u-z)+(2,4)(x-t-z)$$
$$-2z(3,4)+2g_{\mu\nu}(ty+ux-sz)]/3tuxy\,,$$

$$A(4,2) = 8\{-(1,1)st-(2,2)x(s+y+x)-(3,3)zy+(1,2)[s(x+t)+x(u+t)]$$
$$+(1,3)(sz+ty-xu)+(1,4)t(x+y)+(2,3)(zx-ty+xu)-(3,4)zy$$
$$-(2,4)[z(s+2y+x)+y(x+t)+(x-u)x]$$
$$+g_{\mu\nu}x(sz+ty-ux)\}/3txy(s+x+y)\,,$$

$$A(5,2) = 16\{-s(1,2)+(x+y)[(2,3)+(2,4)]\}/3xy(s+x+y)\,,$$

$$A(5,3) = 8(u+y+z)\{(1,1)(t+u)+(2,2)(x+y)-(1,2)(y+u+2z+x+t)$$
$$-z[(1,3)+(1,4)+(2,3)+(2,4)-2sg_{\mu\nu}]\}/3uy(s+t+u)(s+x+y)\,,$$

$$A(7,1) = 12\{-u(1,1)(3s+2x+y)-(2,2)(2sy+sx+2y^2+2xy+2x^2)$$
$$-2(3,3)xu-2(4,4)zx+u(1,3)(y-s-2x)$$
$$+(1,2)[s(-s+2z+2y+x+u-t)+y(2z+y+2x+2u+t)$$
$$+x(4z+u+2t)]+(1,4)(3sz+zy+2zx-2yt+2xu+xt)$$
$$+(2,3)[s(z+2y+2x)+yx+(y+2x)(z+u+2t)]$$
$$+(2,4)(sx+2zy+zx+yx+2yt-2x^2-xu+2xt)$$
$$+(3,4)(z(s+y+x)+2xt)+g_{\mu\nu}(-s^2z+szy+syt+sxu$$
$$-y^2t+3yxu-2x^2u)\}/sxu(s+x+y)\,,$$

$$A(7,2) = 24[(1,2)(-s^2 - sy - 2sx + x^2 - yx) + (2,3)(sy - sx + y^2 + x^2)$$
$$+2(2,4)(sy + sx + y^2 + 2yx + 2x^2)]/sx(s+y+x)^2,$$
$$A(7,7) = 12[(1,2)(s^2 - 9sy - 11sx - 2y^2 - 14yx - 4x^2) + (2,3)(-3sy - 8sx$$
$$+5y^2 - 3yx) + (2,4)(-8sy - 5sx - 5yx + 3x^2)]/s^2(s+y+x)^2,$$
$$A(8,2) = 12[(1,1)(3su - st - yu - yt + xu + xt) + (2,2)(-2sy + sx - 2y^2 - 3yx - x^2)$$
$$-2(3,3)yu - 2(4,4)xt + (1,2)$$
$$\times(-s^2 - 2sz - sy - sx + su + 2zy - 2zx + y^2 + 2yu + 3yt$$
$$-x^2 + 2xu - xt) + (1,3)(sz + 3su + zy - zx - 3yu - xu)$$
$$+(1,4)(-3sz - st + zy - zx + 3yt + xt)$$
$$+(2,3)(-sz + 3zy + zx + y^2 + yx + yu + 3yt)$$
$$+(2,4)(2sz + 2sx + 2zy - yx - x^2 - xu - 3xt) + (3,4)2(yt - sz + xu)$$
$$+g_{\mu\nu}(-3s^2z\text{-}sty + 5sux - sxz - 5syz + txy + ty^2 - ux^2$$
$$-yxu]/sx(s+x+y)(s+u+t),$$
$$A(8,7) = 12\{8s(1,1)(u+t) + 8s(2,2)(y+x) - 8yu(3,3) - 8xt(4,4)$$
$$+(1,2)[s(6s - 16z + y + 3x + u) + t(3s + 14y + 8x) + u(4y + 14x)]$$
$$+(1,3)[s(3u - 8z) + u(3x - 5y)] + (1,4)[s(5t - 8z) + t(5y - 3x)]$$
$$+(2,3)[s(3y - 8z) + y(3t - 5u)] + (2,4)[s(5x - 8z) + x(5u - 3t)]$$
$$+8(3,4)(ty + xu - sz) + 8g_{\mu\nu}s(sz + ty + xu)\}/s^2(s+y+x)(s+u+t).$$

These formulae already include the colour factors. The numbering of the matrix elements exactly corresponds to the order in fig. 1. The other matrix elements are obtained by performing permutations of the momenta. By interchanging momenta p_1 and p_2 we can generate term by term the matrix elements

$$(A(2,1); A(2,2); A(4,2); A(7,1); A(7,2); A(7,7); A(8,2)) \rightarrow$$
$$(A(6,4); A(6,6); A(6,1); A(8,4); A(8,6); A(8,8); A(7,6)).$$

Similarly the interchange of momenta p_3 and p_4 generates new matrix elements

$$(A(1,1); A(2,1); A(2,2); A(3,2); A(4,2); A(5,3); A(7,1); A(7,2); A(8,2)) \rightarrow$$
$$(A(4,4); A(5,4); A(5,5); A(6,5); A(5,1); A(6,2); A(7,4); A(7,5); A(8,5)).$$

The simultaneous interchange of p_1 with p_2 and p_3 with p_4 generates the remaining matrix elements:

$$(A(2,1); A(2,2); A(4,2); A(5,2); A(7,1); A(7,2); A(8,2)) \rightarrow$$
$$(A(3,1); A(3,3); A(4,3); A(6,3); A(8,1); A(8,3); A(7,3)).$$

The calculation of the matrix elements was done in the Feynman gauge. It is then necessary to cancel the contribution from the unphysical gluon polarization by adding ghost diagrams. These appear in the matrix elements $A(7,7)$, $A(8,7)$ and $A(8,8)$. Ghost contributions can of course be avoided by choosing a transverse gauge. However, since the propagator in the transverse gauge contains several terms, the complexity of the matrix elements grow like powers of the number of gluon propagators and become unmanagable even when symbolic computer programs are used. Our cross-section calculations have been done with REDUCE [16].

Appendix B

Analytical leading log calculations

As has been emphasized in the main text, an integration of the order α_s^2 differential cross section over the *whole* phase-space region from the tree-graph contributions alone is not meaningful in massless QCD since one picks up essential singularities from those regions of phase space where off-mass-shell quanta go on-mass-shell. As is well-known, this does not pose any principal difficulty for the theory since these essential singularities are cancelled by the singularities of the α_s^2 virtual one- and two-loop contributions. Meaningful four-jet cross sections are obtained by placing cuts on the integration such that the singular regions are avoided. The so-defined cross sections will then be functions of powers of logarithms of the cut variables. It is the purpose of this appendix to describe somewhat the analytic evaluation of the power and coefficient of the leading log contribution to the two cross sections $e^+e^- \to q\bar{q}gg$ and $e^+e^- \to q\bar{q}q\bar{q}$ for several choices of cut parameters.

The best known of the cut parameters are the (δ, ε) cuts introduced by Sterman and Weinberg [1] which in our context correspond to demanding that any two quanta are separated by at least 2δ in angle and that each quanta carry at least a fraction ε of the total energy. A second possibility to avoid the singular configurations is to place cuts on the invariant mass of pairs and triples of the four produced quanta, i.e, by demanding that $(p_i + p_j)^2 \geqq \hat{\varepsilon} q^2$ and $(p_i + p_j + p_k)^2 \geqq \hat{\varepsilon} q^2$. Finally, the infrared and collinear divergences can be avoided by placing a cut on the topology of the events, i.e., by demanding that the events be acoplanar ($A \geqq A_c$). The various cuts introduced here are sufficient to avoid the singular regions but not always necessary. They do, however, include the whole boundary of the most singular phase-space region yielding the leading log contributions [with the exception of the (δ, ε) cut for $e^+e^- \to q\bar{q}gg$ where the angle cut between the two gluons has to be dropped as discussed in sect. 3).

The Feynman gauge used in the main part of this work is not well-suited for the calculation of the leading log contributions since there are many diagrams contributing at the leading log level. In order to reduce the number of leading log diagrams it is

more convenient to use a physical non-covariant gauge ($n_\mu A^\mu = 0$) with the propagator

$$d_{\mu\nu}(k) = -g_{\mu\nu} + \frac{k_\mu n_\nu + k_\nu n_\mu}{k\cdot n} - n^2 \frac{k_\mu k_\nu}{(k\cdot n)^2}. \tag{B.1}$$

The number of leading log diagrams is further reduced by choosing for n the momentum of the quark (or antiquark) being produced at the electromagnetic vertex [17]: the leading log contributions come only from those diagrams where the (soft and collinear) gluons are emitted from the opposite antiquark (or quark) line.

We take $n = p_2$. The respective leading log diagrams are shown in fig. 8. Diagrams resulting from those in fig. 8 by symmetrizing identical particle legs in the final state (one for $e^+e^- \to q\bar{q}gg$ and three for $e^+e^- \to q\bar{q}q\bar{q}$) are not shown explicitly.

We start with the process $e^+e^- \to q\bar{q}gg$. The leading log contribution to the integrated cross section comes from the region of phase space where the gluons with momenta p_3 and p_4 are soft and approaching collinearity with the quark with momentum p_1. Thus we can neglect terms proportional to p_3 and p_4. Calculating $H_{\mu\nu}$ as defined in (2.3), we obtain in the LLA

$$H_{\mu\nu} = \tfrac{256}{3} g^4 \sum_a Q_a^2 \{p_1, p_2\}_{\mu\nu} \frac{s_{12}^2 s_{13} s_{14}}{s_{134}^3 s_{24} s_{23}} \left[\frac{1}{s_{14}^2} + \frac{1}{s_{13}^2}\right], \tag{B.2}$$

where $s_{ijk} = (p_i + p_j + p_k)^2$, $s_{ij} = (p_i + p_j)^2$.

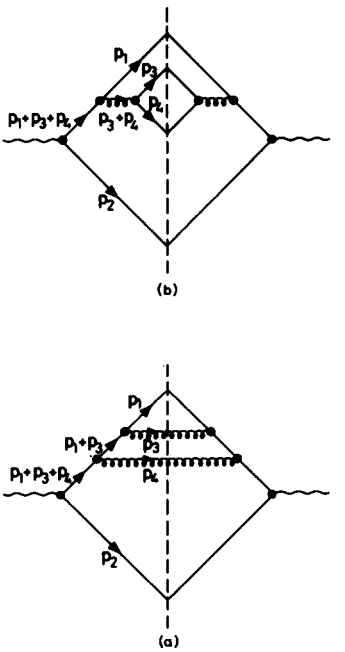

Fig. 8. Leading log diagrams in the transverse gauge ($n = p_2$) for (a) $e^+e^- \to q\bar{q}gg$ and (b) $e^+e^- \to q\bar{q}q\bar{q}$.

The second term in the square bracket of (B.2) results from the symmetrization of gluons with momentum p_3 and p_4. The hadronic tensor (B.2) can be simplified by adding a term $2/s_{14}s_{13}$ to the square bracket in (B.2). This term, which corresponds to fig. 8a but with the gluon lines crossed, contributes only at non-leading level. With this trick we obtain

$$H_{\mu\nu} = \tfrac{64}{3} g^4 \sum_a Q_a^2 \{p_1, p_2\}_{\mu\nu} \frac{(p_1 \cdot p_2)^2}{(p_1 \cdot p_4)(p_1 \cdot p_3)(p_2 \cdot p_4)(p_2 \cdot p_3)} . \tag{B.3}$$

The phase-space integration is considerably simplified at the leading log level by noting that p_3 and p_4 are soft and can be omitted from the energy-momentum δ function. The integration over p_1 and p_2 can be done trivially with the result

$$\int \frac{d^3p_1}{2p_{10}} \frac{d^3p_2}{2p_{20}} \delta^4(q - p_1 - p_2) \{p_1, p_2\}_{\mu\nu} \{p_+, p_-\}^{\mu\nu} = \tfrac{1}{6}\pi q^4 . \tag{B.4}$$

We can now perform the remaining integrations for the various sets of cut parameters.

*(i) Angle-energy (δ, ε) cut**

On substituting angular and energy variables for p_3 and p_4 one finds

$$\sigma_{q\bar{q}gg}^{LLA} = \sigma_0 8 C_F^2 \left(\frac{\alpha_s}{\pi}\right)^2 \ln^2 \delta \ln^2 \varepsilon , \tag{B.5}$$

where $C_F = \frac{4}{3}$. Note that eq. (B.5) is the third term of an exponential series $\sigma_0 \exp(4C_F(\alpha_s/\pi) \ln \delta \ln \varepsilon)$. The cross sections are positive in every order as must be the case, since we are integrating over positive measures. The corresponding cross section for the phase-space integrations *inside* the above boundaries need not be positive definite in every order since virtual gluon graphs also have to be included and, in fact, one finds an exponential series with alternating signs $\sigma_0 \exp(-4C_F(\alpha_s/\pi) \ln \delta \ln \varepsilon)$ [14].

At first sight this is puzzling since one expects the logarithms to cancel when adding the two contributions in the total cross section. However, there are other contributions containing leading logarithms. For example, in 2nd order one has the three-jet contributions, which, at the leading log level, result from the contributions where one gluon approaches the cut boundary from the inside and the other from the outside. There are two of these three-jet contributions with negative signs which cancel the 4- and 2-jet leading logs. A similar reasoning shows that the cancellation of leading logs takes place in every order.

* We would like to acknowledge some useful discussions with J. Stehr.

(ii) Invariant mass ($\hat{\varepsilon}$) cut

It is convenient to use the variables w, x, y and z introduced in [6]. In the space of these variables the remaining integral completely factorizes and one obtains

$$\sigma_{q\bar{q}gg}^{LLA} = \sigma_0 C_F^2 \left(\frac{\alpha_s}{\pi}\right)^2 \tfrac{1}{2} \ln^4 \hat{\varepsilon}\,. \tag{B.6}$$

Using the first order result [6] one again has the first three terms of an exponential series $\sigma_0 \exp(C_F(\alpha_s/\pi) \ln^2 \hat{\varepsilon})$.

(iii) Acoplanarity (A_c) cut

Using the same leading log approximations leading to eqs. (B.3) and (B.4) one finds

$$d\sigma = \sigma_0 C_F^2 (\alpha_s/\pi)^2 \frac{1}{2} \frac{ds_{13}}{s_{13}} \frac{ds_{14}}{s_{14}} \frac{ds_{23}}{s_{23}} \frac{ds_{24}}{s_{24}}\,. \tag{B.7}$$

Since

$$A \propto \min_{i,j(i\neq j)} \{(p_i \cdot p_j)/q^2\}\,, \qquad \text{for } A \to 0\,,$$

this gives

$$\sigma_0^{-1} \frac{d\sigma}{dA} = \tfrac{1}{2} C_F^2 (\alpha_s/\pi)^2 \frac{1}{A} |\ln A|^3\,, \tag{B.8}$$

and on integrating from $A = A_c$

$$\sigma_{q\bar{q}gg}^{LLA} = \sigma_0 C_F^2 (\alpha_s/\pi)^2 \tfrac{1}{8} |\ln A_c|^4\,. \tag{B.9}$$

Next we discuss the process $e^+e^- \to q\bar{q}q\bar{q}$. We do not write down the expression for the hadronic tensor that is obtained from calculating diagram 8b (and its permutations) in the transverse gauge ($n = p_2$) since the result is identical to a similar Feynman-gauge calculation done in [6] except that one has to replace $(N_f - 1)$ in [6] by N_f. Since interference diagrams do not contribute at the leading log level in the transverse gauge it is easy to see that the correct generalization of the non-identical quark calculation in [6] is achieved by the above replacement. There is one subtlety, though. When antisymmetrizing quarks $2 \leftrightarrow 4$ this has to be carried through also in the choice of gauge, i.e., $(n = p_2) \leftrightarrow (n = p_4)$. Although straightforward to calculate, the resulting hadronic tensor $H_{\mu\nu}$ is unwieldy and the necessary integrations are tedious. We only list the results of these calculations

(i) Angle-energy (δ, ε) cut

$$\sigma_{q\bar{q}q\bar{q}}^{LLA} = \sigma_0 C_F^2 N_f (\alpha_s/\pi)^2 \ln^2 \delta |\ln \varepsilon|\,. \tag{B.10}$$

This result is in agreement with the corresponding 3-jet calculation in Smilga and Vysotsky [1].

(ii) Invariant mass ($\hat{\varepsilon}$) cut

$$\sigma^{\mathrm{LLA}}_{\mathrm{q\bar{q}q\bar{q}}} = \sigma_0 C_{\mathrm{F}}^2 N_{\mathrm{f}} (\alpha_{\mathrm{s}}/\pi)^2 \tfrac{1}{2} |\ln^3 \hat{\varepsilon}| \,. \tag{B.11}$$

We have done the acoplanarity integration analytically and find $\sigma^{\mathrm{LLA}}_{(\mathrm{q\bar{q}q\bar{q}})} = \sigma_0 C_{\mathrm{F}}^2 N_{\mathrm{f}} (\alpha_{\mathrm{s}}/\pi)^2 \frac{1}{48} |\ln^3 A_{\mathrm{c}}|$. One notices from fig. 3 that the leading log formula is a gross overestimate of the exact cross section even down to low values of A_{c} indicating that non-leading terms are much more important in the $(\mathrm{q\bar{q}q\bar{q}})$ case than in the $(\mathrm{q\bar{q}gg})$ case. Related to this is the observation that the leading log formula for massive quark production gives a gross overestimate of the exact cross sections even for very large values of $q^2/4m^2$ (see [15] and sect. 4).

Finally, the leading log formula in the massive quark case reads

$$\sigma_{i \neq j} = \frac{4\pi\alpha^2}{q^2} (Q_i^2 + Q_j^2) \left(\frac{\alpha_{\mathrm{s}}}{\pi}\right)^2 \frac{1}{27} \left| \ln^3 \frac{q^2}{4m^2} \right| \tag{B.12}$$

for non-identical quark pair production and

$$\sigma_{ii} = \frac{4\pi\alpha^2}{q^2} Q_i^2 \left(\frac{\alpha_{\mathrm{s}}}{\pi}\right)^2 \frac{1}{27} \left| \ln^3 \frac{q^2}{4m^2} \right| \tag{B.13}$$

for identical quark pair production.

Note that the leading log formula (B.13) in the identical particle case is a factor of 2 smaller than that given in ref. [15] and a factor 2 larger than that of ref. [17]. In the non-identical particle case we agree with the electromagnetic case calculated in [18] after removing the colour factor $\mathrm{Tr}(\frac{1}{2}\lambda_i \frac{1}{2}\lambda_j)\mathrm{Tr}(\frac{1}{2}\lambda_i \frac{1}{2}\lambda_j) = 2$ from (B.12).

Let us close this section with an intuitively obvious remark. The leading singularities in both the $(\mathrm{q\bar{q}gg})$ and $(\mathrm{q\bar{q}q\bar{q}})$ cases multiply the tensor $\{p_1, p_2\}_{\mu\nu}$ in the hadronic tensor $H_{\mu\nu}$ (see (B.3) and [6]). Projecting onto the 6 (helicity) cross sections defined in appendix C one finds that the leading singularity projects only onto σ_{u}. This is not surprising since the leading singularities must appear in the same cross section as the leading 2-loop singularity according to the Lee–Nauenberg argument. The latter obviously only contributes to σ_{u}.

Appendix C

Angular correlations and asymmetries

In case enough hadronic events could be produced with the higher energies of the PETRA and PEP machines, further tests of QCD with four jets in the final states can

be done. In sect. 2 we considered the four-jet cross section integrated over angles θ and χ. Keeping the angular dependence one has:

$$2\pi\frac{d^2\sigma}{d\cos\theta\, d\chi} = \tfrac{3}{8}(1+\cos^2\theta)\sigma_u + \tfrac{3}{4}\sin^2\theta\sigma_L + \tfrac{3}{4}\sin^2\theta\cos 2\chi\sigma_{TR} + \tfrac{3}{4}\sin^2\theta\sin 2\chi\sigma_{TI} + \tfrac{3}{2}\sqrt{\tfrac{1}{2}}\sin 2\theta\cos\chi\sigma_{IR} + \tfrac{3}{2}\sqrt{\tfrac{1}{2}}\sin 2\theta\sin\chi\sigma_{II}\,. \quad \text{(C.1)}$$

The formula (3.1) can be easily derived with the general formalism of Avram and Schiller [19] for angular dependences of multiparticle production in e^+e^- annihilation.

We see that in principle six independent cross sections σ_u, σ_L, σ_{TR}, σ_{TI}, σ_{IR} and σ_{II} can be measured in a 4-jet process. Each of these depend on five variables for which one could choose jet variables as T, $\tilde{S}$, A, etc.

The coordinate system which defines the angles θ and χ in (3.1) can be chosen in different ways depending on which momentum vectors of the final states are used to fix the axes of the coordinate system OXYZ with respect to a system $Oxyz$ with Oz along the beam direction p_+. Let us consider first the genuine four-particle states (2.1) and (2.2). Then a customary choice is the helicity system with OZ along p_1 and OY along the normal to the plane defined by the non-collinear momenta p_1 and p_2. In this frame θ is the polar angle ($0 \leqq \theta \leqq \pi$) and χ the azimuth ($0 \leqq \chi \leqq 2\pi$) which measures the orientation of the XZ plane to the zZ plane. Of course with quarks and gluons being unobservable the final configuration can be specified only by vectors which are determined by hadron momenta in the jets. For example, instead of the momentum vectors p_1 and p_2 we can use the triplicity vectors n_1 and n_2 introduced by Brandt and Dahmen [20]. The above definition of angles θ and χ coincides with the choice B in ref. [11] for describing the orientation of the the three-jet structure. Using some such procedure to define the (θ, χ) orientation of the 4-jet event relative to the beam axis one could then do an angular moment analysis of the experimental distribution (or do an angular polynomial fit) to obtain the 6 cross sections in (C.1).

When calculating the corresponding theoretical distributions one has to exclude the singular regions by placing adequate cuts just as in the angle-integrated case discussed in the main text. The degree of singularity of the 6 cross sections varies from σ_u which contains the most singular contribution down to σ_{TI} which is the least singular. For the same reason σ_u will dominate the other cross sections and thus very accurate measurements would be needed to measure the angular dependences induced by the other non-dominant cross sections.

In practice one could either generate the theoretical angular distributions by Monte Carlo methods and then extract the 6 cross sections using a similar moment analysis as above or one could project a Monte Carlo generated event onto the 6 cross sections on an event-by-event basis. In the latter case the necessary projections would be event-specific and have to be calculated for each event separately.

A less ambitious measurement than the full angular distribution (C.1) would be to determine the distribution of two vectors, for example the thrust vector $\boldsymbol{T}$ and the acoplanarity vector $\boldsymbol{A}$ with respect to the beam direction. For this purpose let θ be the polar angle of $\boldsymbol{T}$ and α the polar angle of $\boldsymbol{A}$ ($0 \leqq \theta \leqq \pi$ and $0 \leqq \beta \leqq \pi$) with the requirement that $\boldsymbol{T} \| \mathrm{OZ}$ and $\boldsymbol{A} \| \mathrm{OY}$. Then $\cos\alpha = \sin\theta \sin\chi$, so that the hemispheres χ and $\pi - \chi$ are not distinguished anymore. If furthermore we do not distinguish between θ and $\pi - \theta$ and α and $\alpha - \pi$ (both are polar angles), respectively, we also lose the contributions which are antisymmetric for $\chi \to \pi - \chi$ in (C.1). Then σ_{TI}, σ_{IR} and σ_{II} drop out in (C.1) and we are left with the following angular distribution:

$$\tfrac{1}{2}\pi\,(\sin\theta - \cos\alpha)^{1/2}\,\frac{\mathrm{d}^2\sigma}{\mathrm{d}\cos\theta\,\mathrm{d}\cos\alpha} = \tfrac{3}{8}(1+\cos^2\theta)\sigma_{\mathrm{u}} + \tfrac{3}{4}\sin^2\theta(\sigma_{\mathrm{L}} + \sigma_{\mathrm{TR}}) - \tfrac{3}{2}\cos^2\alpha\,\sigma_{\mathrm{TR}}\,, \tag{C.2}$$

where now $0 \leqq \theta \leqq \frac{1}{2}\pi$ and $\frac{1}{2}\pi - \theta \leqq \alpha \leqq \frac{1}{2}\pi$. With (3.2) we can still determine three out of the six polarized cross sections which appear in (3.1).

References

[1] G. Sterman and S. Weinberg, Phys. Rev. Lett. 39 (1977) 1436;
P.M. Stevenson, Phys. Lett. 78B (1978) 451;
K. Shizuya and S.-H.H. Tye, Phys. Rev. Lett. 41 (1978) 187;
M.B. Einhorn and B.G. Weeks, Nucl. Phys. B146 (1978) 445;
A.V. Smilga and M.I. Vysotsky, Nucl. Phys. B150 (1979) 173.

[2] G.G. Hanson *et al.*, Phys. Rev. Lett. 35 (1975) 35;
Ch. Berger *et al.*, Phys. Lett. 78B (1978) 176.

[3] J. Ellis, M.K. Gaillard and G. Ross, Nucl. Phys. B111 (1976) 253;
H.D. Politzer, Phys. Lett. 70B (1977) 70B;
T.A. De Grand, Y.J. Ng and S.-H.H. Tye, Phys. Rev. D16 (1977) 3251;
A. De Rújula, J. Ellis, E.G. Floratos and M. K. Gaillard, Nucl. Phys. B138 (1978) 387;
G. Kramer and G. Schierholz, Phys. Lett. 82B (1979) 82B;
G. Curci, M. Greco and Y. Srivastava, Nucl. Phys. B159 (1979) 451.

[4] P. Söding, Talk at the EPS-Meeting, Geneva, July, 1979;
H. Newman, Talk at the Photon-hadron conference, Chicago, August, 1979.

[5] S.-Y. Pi, R.L. Jaffe and F.E. Low, Phys. Rev. Lett. 41 (1978) 142;
G. Kramer, G. Schierholz and J. Willrodt, Phys Lett. 78B (1978) 249 (E: 80B (1979) 433);
C.L. Basham, L.S. Brown, S.D. Ellis and S.T. Love, Phys. Rev. D17 (1978) 2298.

[6] T.A. De Grand, Y.T. Ng and S.-H.H. Tye, Phys. Rev. D16 (1977) 3251.

[7] A. De Rújula *et al.*, ref. [3].

[8] A. Ali, J.G. Körner, G. Kramer and J. Willrodt, Z. Phys. C1 (1979) 203.

[9] A. De Rújula, R. Petronzio and B. Lautrup, Nucl. Phys. B146 (1978) 50;
K. Koller, T.F. Walsh and P.M. Zerwas, Phys. Lett. 82B (1979) 263.

[10] A. Ali, J.G. Körner, Z. Kunszt, J. Willrodt, G. Kramer, G. Schierholz and E. Pietarinen, Phys. Lett. 82B (1979) 285.

[11] G. Kramer *et al.*, ref. [5].

[12] R.D. Field and R.P. Feynman, Nucl. Phys. B136 (1978) 1.

[13] A. Ali, J.G. Körner, G. Kramer and J. Willrodt, DESY preprint 79/63 (1979); Nucl. Phys. B, to be published.

[14] E. Curci and M. Greco, Phys. Lett. 79B (1978) 406;
A.V. Smilga, Phys. Lett. 83B (1979) 357.
[15] G.C. Branco, H.P. Nilles and K.H. Streng, Phys. Lett. 85B (1979) 269; and references therein.
[16] A.C. Hearn, Stanford University Report No. ITP-247.
[17] W. Furmanski, R. Petronzio and S. Pokorski, Nucl. Phys. B155 (1979) 253.
[18] V.N. Baier, V.S. Fadin and V.A. Khoze, JETP (Sov. Phys.) 23 (1966) 104.
[19] N.M. Avram and D.H. Schiller, Nucl. Phys. B70 (1974) 272.
[20] S. Brandt and H.D. Dahmen, Z. Phys. C1 (1979) 61.